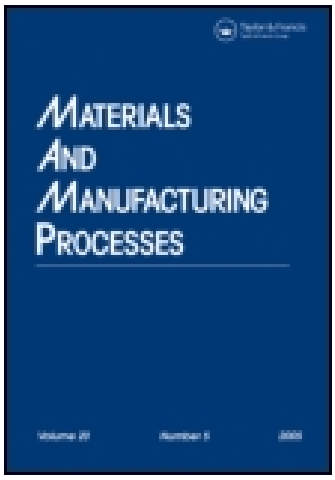

Materials and Manufacturing Processes
Publication details, including instructions for authors and subscription information:
http://www.tandfonline.com/loi/lmmp20

Foil Optimization in Tailor Welded Blank of an Automotive Floor Component

K. Hariharan [a] , K. Kalaivani [a] & G. Balachandran [a]
[a] Advanced Engineering , Ashok Leyland Ltd. , Chennai , India
Accepted author version posted online: 03 Oct 2011.Published online: 01 Aug 2012.

To cite this article: K. Hariharan , K. Kalaivani & G. Balachandran (2012) Foil Optimization in Tailor Welded Blank of an Automotive Floor Component, Materials and Manufacturing Processes, 27:9, 936-942, DOI: 10.1080/10426914.2011.610077

To link to this article: http://dx.doi.org/10.1080/10426914.2011.610077

Materials and Manufacturing Processes, 27: 936–942, 2012

ISSN: 1042-6914 print/1532-2475 online
DOI: 10.1080/10426914.2011.610077

Taylor & Francis
Taylor & Francis Group

Foil Optimization in Tailor Welded Blank of an Automotive Floor Component

K. Hariharan, K. Kalaivani, and G. Balachandran

Advanced Engineering, Ashok Leyland Ltd., Chennai, India

In the present work, double foil butt resistance seam welding in an automotive floor component has been investigated. The possibility of reducing foil from the existing configuration is evaluated. Mechanical properties of the single and double foil weld configuration are compared using tensile tests. The fractography of failed location is analyzed, and the force distribution in base metal and welded specimen is derived analytically to explain the observations in tensile tests. The microstructure and hardness profile of both the weld configurations and their influence on the mechanical properties are analyzed. The weld defect is analyzed using ultrasonic inspection technique. Based on the evaluation of metallurgical characterization and mechanical properties evaluation, the number of foils in an automotive floor component has been optimized. Cost savings of around 30% in the welding process is achieved by foil optimization.

Keywords Erichsen cup test; Fractography; NDT; Optimization; Seam welding; Ultrasonic inspection.

Introduction

Tailor welded blanks (TWBs) find increasing application in automotive industry for reducing weight and cost [1]. Manufacturing of TWB involves welding optimal combination of different material grades and thicknesses prior to forming to maximize the strength/weight ratio of the sheet metal component. The welding process affects the mechanical properties of the TWBs [2]. It is observed that the welding process reduces the ductility of TWBs. The reduction in ductility of TWBs depends on several factors, such as the welding process [3], specimen size [4], base material being welded [5], weld line orientation [6], and thickness ratio [7]. The tensile strength of the TWBs is almost in the same order of base metal [3, 6–8] with the exception of certain materials like hardened aluminium alloys, where the weld strength is less than the base metal [9, 10]. However, this is in contrast with a few works where appreciable difference in strength is observed between the welded and base metal specimens [11, 12]. The hardness of the welded zone generally increases due to welding. The increase in hardness in the welded zone depends upon the base metal [13], welding process [14], and thickness ratio [7]. The variation of hardness profile due to welding process is attributed to the heat input during welding [14]. The inhomogenity of microstructure and mechanical properties caused by the weld affects the formability of welded blanks. The formability of welded blanks depends upon the material combination [5], weld line orientation [15], thickness ratio [16], and welding process [14].

Extensive work on welded blanks have been carried out using laser welding process, primarily due to its flexibility in joining sheets of different thicknesses and nonlinear weld line. However, when the sheets to be joined are of the same thickness, resistance seam welding process is a cost effective alternative solution. The heat input and cooling rate of resistance welding is lesser than that of laser welding, resulting in reduced formation of martensite. Therefore, resistance welding exhibits better formability than laser welding [17]. Saunders and Wagoner [14] observed mash seam welding to exhibit higher ductility with lower weld hardness when compared to laser welding.

The principle of resistance seam welding is similar to spot welding. Similar to spot welding [18, 19], heat input to seam welding process [20] depends on the weld current, weld time, and electrode force. Mash seam welding and foil butt seam welding are applicable to thin sheet metal applications [20]. Mash seam welding involves local deformation and diffusion of the lapped interface at high temperature. This causes local distortion at the weld interface [20, 21]. In a foil butt seam welding, the sheet metals to be joined are butted against the interface, and a thin foil strip is fed between the sheet and electrode wheel. The foil assists in distributing the weld current to both the sheets. The distortion of the weld interface in foil butt seam welding is negligible when compared to mash seam welding [21]. However, literature on foil butt resistance seam welding is scarce.

The present study focuses on optimization of seam weld foil in an automotive floor component. The input blank of the floor component is prepared by seam welding two 1.2 mm thick interstitial free (IF) grade steel sheets. At the end of initial draw, the weld line is trimmed

Received March 7, 2011; Accepted July 17, 2011

Current affiliation for G. Balachandran: Kalyani Carpenter Special Steels Ltd., Pune, India.

Address correspondence to K. Hariharan, Advanced Engineering, Ashok Leyland Ltd., Chennai 600 103, India; E-mail: hariharan.k@ashokleyland.com

off and the subsequent operations are performed without weld joint. In a typical foil butt seam welding, around 63% [22] of the manufacturing cost is due to foils. Eliminating one foil can bring down the welding cost by around 30%. The functional requirement of the seam weld joint in the floor component is to withstand the load during initial forming process. As the weld joint is not a part of final component, fatigue properties of welded joint need not be considered for optimization. The mechanical and metallurgical properties of single and double foil seam weld configurations are studied, and the number of foils in the weld process is optimized based on characterization.

Experimental work

The present study is carried out using commercially available 1.2 mm thick IF sheets (Table 1). Seam welding (machine make: Messer Greishem) using single foil and double foil is carried out (weld parameters: 200 A current, 2 bar roller pressure, 2 m/min feed rate).

The microstructure of weld sections were studied using an optical microscope. The hardness profile across weld sections were determined using Vicker's hardness machine (machine make: Zwick/Roell) at a load of 1,000 grams. The fracture region was studied using a scanning electron microscope (machine make: Quanta).

Ultrasonic inspection of single and double foil seam welds was performed by immersion pulsed echo method using a 10 MHz piezoelectric transducer. The transducer and specimen were completely immersed in water (couplant).

Tensile testing of IF base metal samples (along three directions, 0^{o}, 45^{o}, and 90^{o}) were performed as per ASTM E8 standard. Plastic strain ratio tests on IF base metal specimens were carried out as per ASTM E517 along the three directions mentioned above for tensile testing. The typical failure mode observed in the considered component is along weld transverse direction (Fig. 1). Hence, transverse welded specimens were evaluated for mechanical properties. Transverse tests evaluate the strength of weld joint against the base metal [23].

Erichsen cup tests were carried out in base metal, single foil, and double foil seam welded specimens. All the tests were performed in dry lubrication condition. The deformation height before failure is noted.

Results and discussion

The mechanical and metallurgical characteristics of single and double foil weld specimen are compared with that of base metal sample.

Table 1.—Chemical composition of base metal and foil used for the study.

(%)	C	Mn	S	P	Al	Si	Others
IF	0.002	0.155	0.007	0.009	0.027	0.007	Nb-0.001 Ti-0.033 V-0.028
Foil	0.057	0.216	0.007	0.011	0.029	0.009	

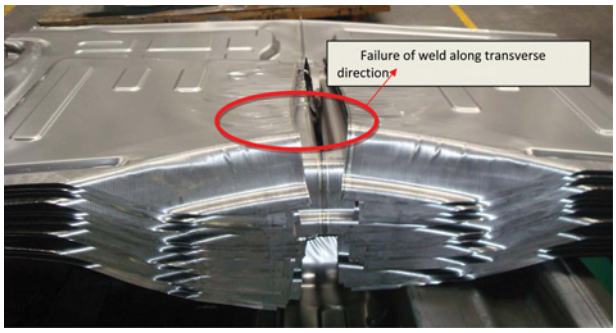

Figure 1.—Formed floor component indicating failure along transverse direction (color figure available online).

Microstructure and Hardness Distribution

The hardness profile of both single and double foil (Fig. 2) is similar, with marginally higher hardness for double foil material. The increase in hardness of double foil specimen is due to the additional heat input from the second foil. The carbon content in the foil material also contributes to the increment in hardening. The ratio of hardness increment in the fusion zone with respect to base metal hardness is around 50 to 60%, which is higher than the values reported [14] for mash seam welding. The difference is attributed to the microstructural characteristics of mash seam welding and foil-butt seam welding.

The microstructure constituents of both single and double foil welds were similar. The microstructure of the weld cross-section reveals fine grains in the foil region and good bonding between foil and base metal (Fig. 3). The fusion zone of both single and double foil (Fig. 3) weld section is characterized with a mixture of coarse and fine ferrite grains with fine ferrite along the grain boundary of allotriomorphic ferrite [24]. The heat-affected zone (HAZ) is characterized with large ferrite grains elongated along the direction of heat flow. The excessive grain growth observed in the HAZ zone is due to higher amplitude of thermal gradient [25], which increases from the fusion zone towards base metal.

It is observed in the single foil weld that the diffusion bonding is incomplete in the foil-free side causing a

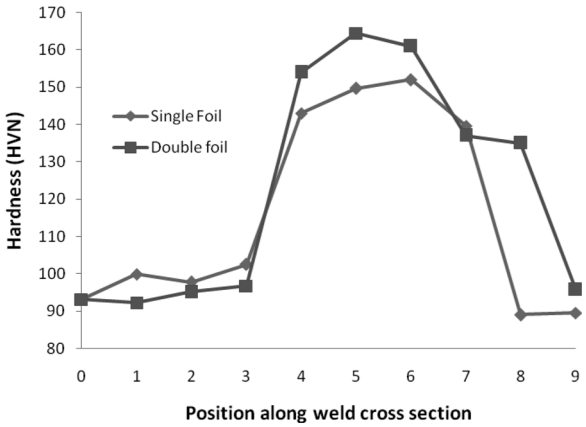

Figure 2.—Hardness profile of single and double foil welded specimen.

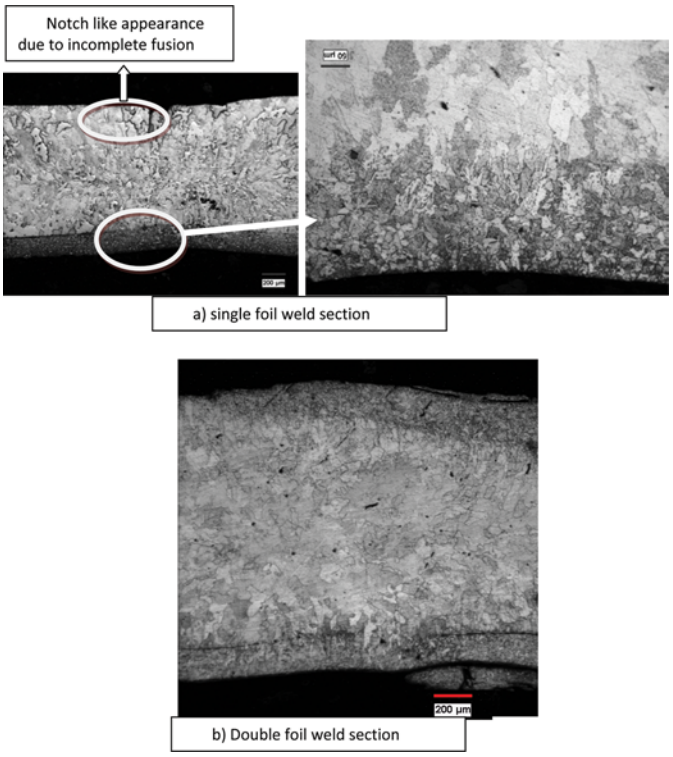

FIGURE 3.—Microstructure of single and double foil welded specimen (color figure available online).

notch-like appearance (Fig. 3), which can potentially cause premature tensile or fatigue failure. In the case of double foil weld, foil penetrates from both top and bottom sheet surfaces allowing sufficient diffusion.

Ultrasonic inspection of single foil weld is performed to check whether the defect is localized or continuous. The C-scan in Fig. 4 shows the top most layer of single foil weld specimen. A section of B-scan intersects the foil center where the notch-like defect was observed in the microstructure. The B-scan image in the right side of Fig. 4 displays no signal in the foil center position indicating lack of material for reflection. Thus the notch-like defect observed in the microstructure is continuous throughout the weld line.

Further inspection of single foil and double foil specimen using C-scan image confirms the presence of continuous defect in single foil specimen (Fig. 5). It is observed that the amplitude of reflected sound energy is lower in the weld region of double foil specimen when compared to single foil specimen. This indicates that the sound wave has propagated through a larger distance in double foil weld than single foil weld. This is due to the additional thickness caused by the presence of second foil in the double foil weld.

In the case of single foil welded specimen, the central portion of the weld foil exhibits (Fig. 5) higher amplitude of reflected wave than the base plate. The incomplete diffusion bonding of single foil welded causes a continuous line defect, which allows earlier reflection of sound wave when compared to other weld and base metal region.

Interpretation from Tensile Test

The yield strength of single and double foil welded specimens is almost the same (Fig. 6), though slightly higher than that of the base metal.

The failure of single and double foil specimen occurred in base metal, indicating that the weld is stronger in both the cases. The tensile properties of base metal and welded samples are given in Table 2.

The fractography of the failed location in base metal specimen and double foil welded specimen (Fig. 7) are characterized by dimples indicating ductile mode of failure. The flat failure zone of base metal was characterized with smaller and shallow voids, whereas the failure zone of double foil welded specimen is characterized with relatively larger and deep voids. The width of the distinct flat failure zone was largest in base metal specimen and gradually decreased in single foil specimen and was

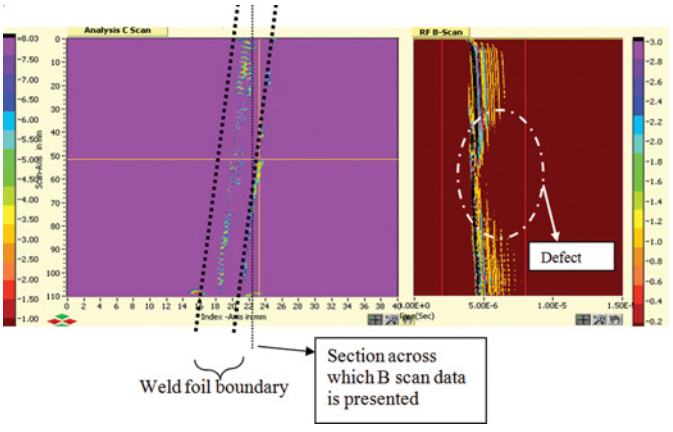

FIGURE 4.—B-scan image (right) indicates the location of defect. C-scan image (left) displays the foil position and the section of B-scan image (color figure available online).

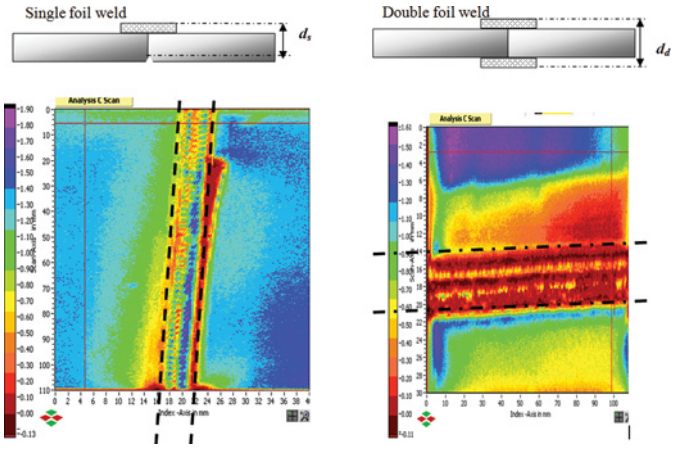

FIGURE 5.—C-scan image of single and double foil welded specimen (color figure available online).

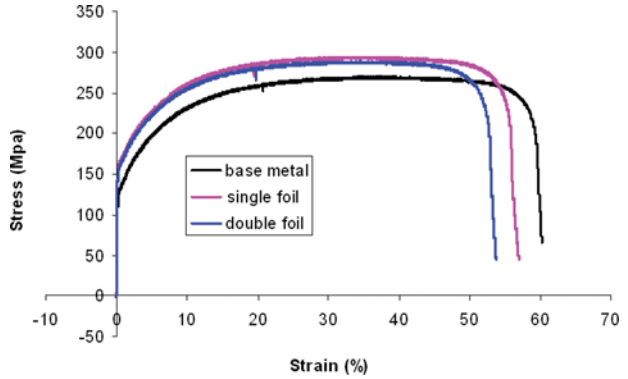

FIGURE 6.—Stress-strain curve of base metal and welded samples (color figure available online).

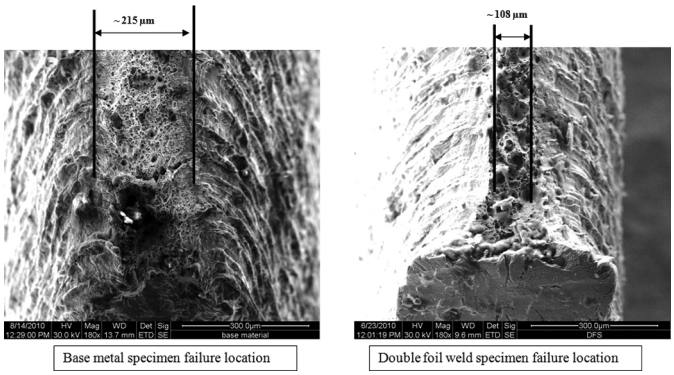

FIGURE 7.—Fractography of base metal (180×) and double foil weld sample (failure zone is base metal) 180×.

negligible in the double foil specimen This indicates that the load distribution of welded specimen is different from that of base metal.

To understand the failure behavior observed in welded specimen, double foil weld configuration is analyzed analytically. The weld region post tensile testing can be divided into three zones as schematically shown in Fig. 8.

Zone I refers to the central rigid weld region with no deformation along width and thickness direction. Zone III is the base metal away from weld zone whose deformation behavior is similar to the base metal specimen. Zone II is the intermediate transition zone where the strain increases gradually.

In the case of zone I, the rigid weld region constrains material flow in width and thickness directions. Therefore, the strain along width and thickness is zero in zone I.

$$\varepsilon_y = \varepsilon_z = 0,$$

where x, y, and z are along the directions length, width, and thickness of the tensile specimen.

Assuming isotropic material behavior,

$$\varepsilon_y = \frac{\sigma_y}{E} - \frac{\upsilon\sigma_x}{E} - \frac{\upsilon\sigma_z}{E}; \varepsilon_z = \frac{\sigma_z}{E} - \frac{\upsilon\sigma_x}{E} - \frac{\upsilon\sigma_y}{E}$$

where x, y, and z are length, width, and thickness directions, respectively.

Since zone I is rigid, $\varepsilon_{width} = \varepsilon_{thickness} = 0$, we get $\sigma_y = \sigma_z$.

Substituting in expression of ε_y, $\sigma_y = \sigma_z = \frac{\upsilon}{(1-\upsilon)}\sigma_x$, ($\upsilon$ indicates effective Poisson's ratio accounting elastic-plastic conditions). Therefore, the additional loads acting on a double foil welded specimen is given as

$$\therefore (P_y)_{zoneI} = \frac{\upsilon}{(1-\upsilon)}\sigma_x(l_I w_o); (P_z)_{zoneI} = \frac{\upsilon}{(1-\upsilon)}\sigma_x(l_I t_o),$$

where P_y, P_z indicates additional loads acting in width and thickness directions, l_I, w_o, and t_o indicates length, initial width, and initial thickness of zone I.

The strain along width and thickness direction increases gradually from zero in zone I to maximum in zone III through zone II. Approximating the strain variation as sinusoidal function, $\varepsilon = \varepsilon_{\max} Sin\frac{\pi x}{4a}$, where 'a' indicates the size of zone II along the length of specimen. Strain distribution is symmetric with respect to zone I; therefore, total strain in zone II is

$$\varepsilon_{tot} = 2\int_0^a \varepsilon.dx = 2\int_0^a \varepsilon_{\max} Sin\frac{\pi x}{4a}dx.$$

TABLE 2.—Mechanical properties of base metal and welded samples.

	Yield strength (Mpa)	Tensile strength (Mpa)	Elongation (%)	n	Rbar
Base metal	152.46	290.75	60.14	0.29	1.99
Single foil	164	294	56.43	0.28	
Double foil	159	288.52	53.23	0.28	

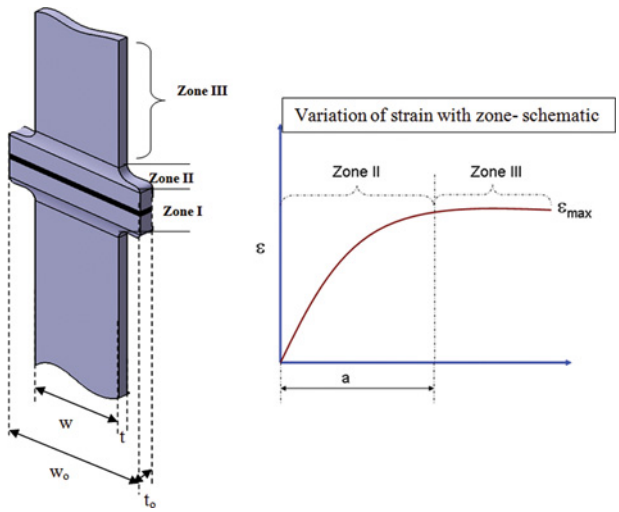

FIGURE 8.—Double foil tensile specimen after testing (schematic) (color figure available online).

Integrating, $\varepsilon_{tot} \cong 0.746 \cdot a\varepsilon_{\max}$.

The additional load induced by the strain in zone II is given as

$$(P_y)_{zoneII} = (\sigma_y)_{zoneII} \int_0^a dA_y = 0.746 \cdot E \cdot a \cdot (\varepsilon_y)_{\max} \int_0^a dA_y$$

$$(P_z)_{zoneII} = (\sigma_z)_{zoneII} \int_0^a dA_z = 0.746 \cdot E \cdot a \cdot (\varepsilon_z)_{\max} \int_0^a dA_z.$$

The total additional load in the welded specimen due to zone I and zone II is given as

$$P_y = \frac{\upsilon}{(1-\upsilon)} \sigma_x (l_I w_o) + 0.746 \cdot E \cdot a \cdot (\varepsilon_y)_{\max} \int_0^a dA_y$$

$$P_z = \frac{\upsilon}{(1-\upsilon)} \sigma_x (l_I t_o) + 0.746 \cdot E \cdot a \cdot (\varepsilon_z)_{\max} \int_0^a dA_z.$$

This additional load induces additional shear stresses in the tensile specimen along the tensile axis, which explains the reduced flat plateau region observed in the failure zone of welded tensile specimen.

The presence of additional shear stress is complemented by the fractography of base metal and double foil weld. As noted earlier, the approximate void size in the failure zone of double foil specimen is larger than that of base metal specimen. Narayanaswamy and Sathiyanarayanan [26] have correlated the increase in void size with increase in shear strain (stress). The increase in void size in the double foil specimen is due to the additional shear stress induced by the weld constraints.

Interpretation from Erichsen Cup Tests

The ductility in uniaxial strain mode does not guarantee sufficient ductility in other strain modes like plane strain mode or biaxial stretching. The Erichsen cupping test stretches the material biaxially and the cup height at the onset of failure is an indicator of formability (Fig. 9). It was observed that the formability of single foil welded specimen was marginally superior to double foil weld specimen (87.6% against 84.5% of the base metal). The reduced ductility observed in the double foil weld specimen is attributed to the additional constraint imposed by the second foil. The formed Erichsen cup was sectioned and the variation of thickness was measured in specific locations (Fig. 9). The failure location is indicated by location '3' and is slightly offset from the apex due to friction [27]. The variation of thickness with location is plotted in Fig. 9. At the apex point, the thicknesses of both single and double foil specimen were similar indicating negligible deformation. This is in line with the assumption made in deriving the stress distribution in double foil specimen. The thickness at apex point in base metal was less than the welded specimen, indicating plastic deformation. The thickness at failure location was least for base metal, followed by single foil specimen and double foil specimen. This indicates maximum deformation in base metal and least deformation in double foil specimen, due to the additional constraints explained above. During plastic deformation

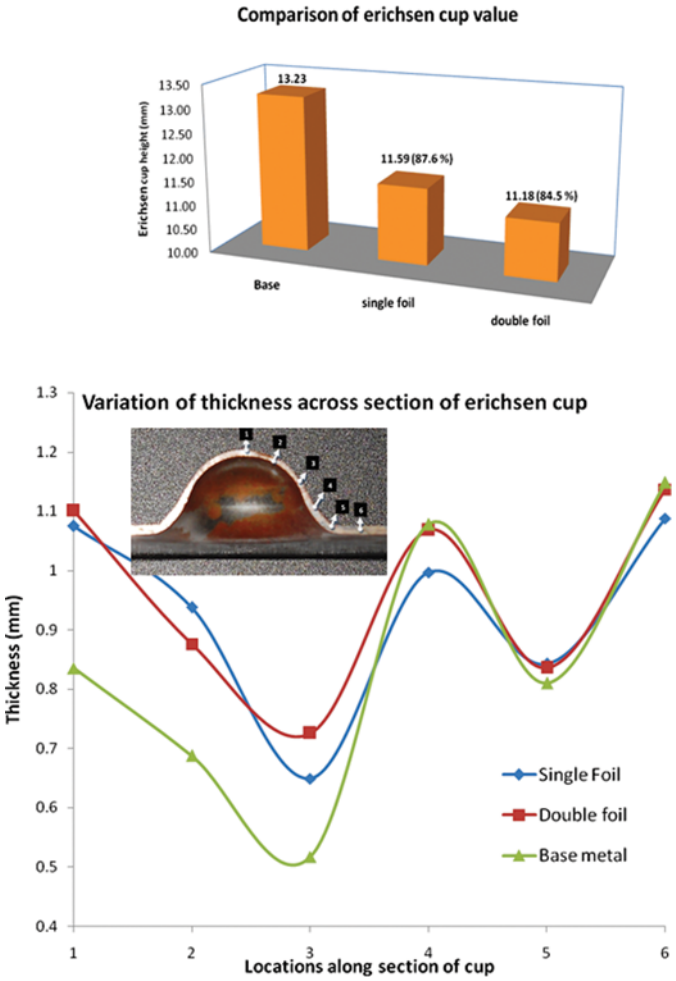

FIGURE 9.—Comparison of Erichsen cup height for base metal and weld specimen (top); variation of thickness across specified locations in the section of Erichsen cup (bottom) (color figure available online).

of cup, the metal is bent across the shoulder radius causing reduction in thickness near location '5.'

IMPLEMENTATION OF SINGLE FOIL WELDED SHEET METAL BLANKS FOR FLOOR COMPONENT

It is inferred from the microstructure and ultrasonic inspection that single foil welded sheet has a potential stress concentration zone due to weld line defect. However, the tensile test results with weld line transverse to loading direction revealed no appreciable difference in the strength. This indicates that single foil seam welded sheet is sufficient to meet the requirements when the weld line is transverse to the loading direction. In the case of sheet metal components, the loading is multiaxial in nature and the major strain direction can be considered as loading direction. The weld line of automotive floor component considered in the present study is perpendicular to the major strain direction and the inference of tensile results is applicable to component. The weld line acts as a local constraint for metal flow; the double

foil weld configuration is constrained at both the sides whereas the single foil weld specimen is constrained at only on side. Hence, the ductility and formability of single foil welded specimen is marginally superior to double foil specimen. This is confirmed from the observations of Erichsen cup test. Thus based on the observations, it is inferred that single foil weld configuration is sufficient to meet the requirements of the input blank.

A batch of around 500 sheet metal blanks was welded with single foil configuration and formed using existing tools. Forming behavior of single foil welded blanks was observed to be similar to that of double foil welded blanks.

Based on the initial pilot trials, single foil configuration has been implemented in regular production. The optimized welding configuration with single foil resulted in a cost savings of around 30% of the welding cost.

Conclusion

Based on the comparative evaluation, the following conclusions are arrived at:

1. Tensile strength along transverse direction to weld axis is similar for both single and double foil weld configurations.
2. Microstructure and ultrasonic testing revealed a potential stress concentration zone in the single foil weld configuration. However, the weld strength was higher than that of base metal and hence did not affect the mechanical properties.
3. The tensile behavior of the weld specimens were interpreted using fractography images and a plausible analytical explanation is derived.
4. Single foil weld configuration implemented in the floor component resulted in cost savings of around 30% in welding process.

Acknowledgments

Authors would like to thank Ms. Abilasha, Ph.D. scholar, IIT Madras for her assistance in ultrasonic weld inspection. Authors would like to acknowledge Mr. Praveen (CPPS), Mr. Sathyanarana Rao (CPPS), and Mr.Anand (CTL) of Ashok Leyland for their assistance in sample preparation and testing.

References

1. Jiang, H.M.; Li, S.H.; Wu, H.; Chen, X.P. Numerical simulation and experimental verification in the use of tailor-welded blanks in the multi-stage stamping process. *Journal of Materials Processing Technology* **2004**, *151*, 316–320.
2. Zadpoor, A.A.; Sinke, J.; Benedictus, R. Mechanics of tailor welded blanks: An overview. *Key Engineering Materials* **2007**, *344*, 373–382.
3. Miles, M.P.; Nelson, T.W.; Decker, B.J. Formability and strength of friction-stir-welded aluminum sheets. *Metallurgical and Materials Transactions A* **2004**, *35*, 3461–3468.
4. Ghoo, B.Y.; Keum, Y.T.; Kim, Y.S. Evaluation of mechanical properties of welded metal in tailor welded steel sheet welded by CO_2 laser. *Journal of Material Processing Technology* **2001**, *113*, 692–698.
5. Panda, S.K.; Ravikumar, D. Experimental and numerical studies on the forming behavior of tailor welded steel sheets in biaxial stretch forming. *Materials and Design* **2010**, *31*, 1365–1383.
6. Cheng, C.H.; Chan, L.C.; Chow, C.L.; Lee, T.C. Experimental investigation on the weldability and forming behavior of aluminum alloy tailor-welded blanks. *Journal of Laser Applications* **2005**, *17*, 81–89.
7. Chan, L.C.; Cheng, C.H.; Chan, S.M.; Lee, T.C.; Chow, C.L. Formability analysis of tailor-welded blanks of different thickness ratios. *Journal of Manufacturing Science and Engineering* **2005**, *127*, 743–751.
8. Min, K.B.; Kim, K.S.; Kang, S.S. A study on resistance welding in steel sheets using a tailor-welded blank (1st report): Evaluation of upset weldability and formability. *Journal of Materials Processing Technology* **2000**, *101*, 186–192.
9. Stasik, M.C.; Wagoner, R.H. Forming of tailor-welded aluminum blanks. In *Aluminium and Magnesium for Automotive Applications*; Bryant, J.D., Ed.; TMS: Warrendale, PA, 1996; 69–83.
10. Xia, C.; Li, M.; Perrusquia, N.; Mao, S.X. Interfacial structure and micro and nano-mechanical behavior of laser-welded 6061 aluminum alloy blank. *Journal of Engineering Materials and Technology* **2004**, *126*, 8–13.
11. Abdullah, K.; Wild, P.M.; Jeswiet, J.J.; Ghasempoor, A. Tensile testing for weld deformation properties in similar gage tailor welded blanks using the rule of mixtures. *Journal of Materials Processing Technology* **2001**, *112*, 91–97.
12. Panda, S.K.; Ravi Kumar, D.; Harish, K.; Nath, A.K. Characterization of tensile properties of tailor welded IF steel sheets and their formability in stretch forming. *Journal of Materials Processing Technology* **2007**, *183*, 321–332.
13. Bayraktar, E.; Kaplan, D.; Yilbas, B.S. Comparative study: Mechanical and metallurgical aspects of tailored welded blanks (TWBs). *Journal of Material Processing Technology* **2008**, *204*, 440–450.
14. Saunders, F.I.; Wagoner, R.H. Forming of tailor-welded blanks. *Metallurgical and Materials Transactions A* **1996**, *27*, 2605–2616.
15. Narayanan, R.G.; Narasimhan, K. Predicting the forming limit strains of tailor-welded blanks. *The Journal of Strain Analysis for Engineering Design* **2008**, *43*, 551–563.
16. Chan, S.M.; Chan, L.C.; Lee, T.C. Tailor-welded blanks of different thickness ratios effects on forming limit diagrams. *Journal of Materials Processing Technology* **2003**, *132*, 95–101.
17. Meinders, T.; Berg, A.V.; Huetink, J. Deep drawing simulations of tailored blanks and experimental verification. *Journal of Materials Processing Technology* **2000**, *103*, 65–73.
18. Aslanlar, S.; Ogur, A.; Ozsarac, U.; Ilhan, E. Welding time effect on mechanical properties of automotive sheets in electrical resistance spot welding. *Materials and Design* **2008**, *29*, 1427–1431.
19. Ozyurek, D. An effect of weld current and weld atmosphere on the resistance spot weldability of 304 L austenitic stainless steel. *Materials and Design* **2008**, *29*, 597–603.
20. Michael, J.K. Resistance seam welding. In *ASM Handbook*. Volume 6, Welding Brazing and Soldering. ASM International: Materials Park, OH, 1993.
21. Dent, P.; Bohr, J.C.; Gasser, R.G.; Gerken, J.M.; Hallum, D.L.; Lee, J.W.; McCauley, R.B.; Orts, D.H.; Oyler, G.W.;

Shieh, W.T.; Wu, K.C.; Manz, A.F. Welding processes. Chapter 17, Volume-2 of *Welding Handbook*. American Welding Society: Miami, FL, **1997**.
22. Costing department. Ashok Leyland. Internal communication, 2010.
23. Panda, S.K.; Ravi Kumar, D.; Harish, K.; Nath, A.K. Characterization of tensile properties of tailor welded IF steel sheets and their formability in stretch forming. *Journal of Materials Processing Technology* **2007**, *183*, 321–332.
24. Bhadeshia, H.K.D.H.; Honeycombe, R.W.K. *Steels Microstructure and Properties*; Butterworth-Heinemann: Oxford, UK, **2006**.
25. Bayraktar, E.; Kaplan, D.; Devillers, L.; Chevalier, J.P. Grain growth mechanism during the welding of interstitial free (IF) steels. *Journal of Materials Processing Technology* **2007**, *189*, 114–125.
26. Narayanasamy, R.; Sathiya Narayanan, C. Forming limit diagram for Indian interstitial free steels. *Materials and Design* **2006**, *27*, 882–899.
27. Hariharan, K.; Prakash, R.V.; Sathya Prasad, M. Influence of yield criteria in the prediction of strain distribution and residual stress distribution in sheet metal formability analysis for a commercial steel. *Materials and Manufacturing Processes* **2010**, *25*, 828–836.